ISSN 2517-8008
THE SOCIETY FOR EARTHQUAKE AND
CIVIL ENGINEERING DYNAMICS

NEWSLETTER

Volume 30 No 1
April 2019

In this issue

Smart Wireless Sensors for Energy-Efficient Structural Health Monitoring

Kyriaki Gkoktsi
AKTII, London, UK

Abstract

This article presents a novel sub-Nyquist spectral estimation approach that can be embedded into smart wireless sensors for low-power structural health monitoring applications. The proposed method, termed multi-sensor power spectrum blind sampling approach, relies on arrays of wireless sensors that operate in a deterministic non-uniform in time-domain multi-coset sampling scheme, capable of acquiring compressed structural acceleration response signals at sampling rates below Nyquist. The acquired compressed measurements are transmitted to a central server and collectively processed using a power spectrum blind sampling (PSBS) technique to estimate the power spectrum density matrix of the acceleration responses. Acceleration measurements are treated as realisations of a stationary random process without making any assumption on the signal structure (e.g., sparsity). Structural modal properties are then extracted through standard frequency domain decomposition (FDD). The efficacy of the proposed approach is numerically assessed at a high signal compression level using field-recorded data obtained from a monitored bridge in Zürich, Switzerland. It is shown that accurate mode shapes can be obtained from 89% fewer measurements compared to conventional non-compressive FDD, leading to significant energy gains within battery-operated wireless sensors. It is envisaged that the proposed multi-sensor PSBS approach would support more sustainable long-term wireless structural health monitoring systems once sensors with multi-coset sampling capabilities become commercially available.

Editors' note: On 31st October 2018, Dr Kyriaki Gkoktsi (AKTII) presented her work during an event organised by the SECED Young Members' Group. The event, hosted at the Institution of Civil Engineers, was on Vibration, Offshore, and Blast Engineering. Kyriaki provided the following article presenting aspects of her research work on operational modal analysis and signal processing.

1. Introduction

Vibration-based Structural Health Monitoring (VSHM) of civil engineering structures aims to assess their structural integrity and performance either periodically or following extreme events/actions (e.g., Brownjohn, 2007). VSHM relies on acquisition and processing of excitation (input) and structural response (output) signals measured by sensors placed on structures for the purpose of (*i*) estimating the inherent dynamic/modal properties of linearly vibrating structures under operational conditions, and (*ii*) detecting potential structural damage. In this context, the *operational modal analysis* (OMA) framework (e.g., Brincker and Ventura, 2015) utilises unmeasured ambient/natural excitation forces; these are assumed to be stationary broadband random processes and can be approximated as white noise. OMA is suitable for real-time monitoring of large-scale and complex structures minimising cost and network disruption, while being particularly useful in cases where it is difficult or unaffordable to measure the input forces, and/or when controllable excitation of structures is not feasible in practice.

Over the last two decades, the consideration of *wireless sensor networks* has been an important development in VSHM of civil structures (e.g., Lynch, 2007). It has emerged as a viable alternative to cabled sensor networks which are restricted by costly and labour-intensive installations of long coaxial wires. Specifically, wireless sensor networks enable dense structural instrumentation and access to remote locations on structures, offering rapid, less obtrusive, and more economical VSHM implementations, especially in monitoring large-scale and geometrically complex civil engineering structures. However, the above advantages are counterbalanced by costly requirements in the power supply of networks. Power requirements can be met either with expensive energy harvesting strategies or with battery operated wireless sensors of increased maintenance cost (i.e., frequent battery replacement depending on factors such as the sampling frequency, the duration of each monitoring interval, and the on-board hardware and software code to be executed). Power requirements are further increased due to wireless data transmission, which is the most power-hungry operation in battery operated wireless sensor networks (Lynch, 2007).

To address the above issues, various researchers have recently considered compressive sensing-based (CS) techniques for OMA aiming to reduce the energy consumption of sensors by considering random *sub-Nyquist* sampling rates at the analog-to-digital converter units, and, at the same time, reduce the data transmitted within wireless sensor networks (e.g., O'Connor et al., 2014; Park et al., 2014; Yang and Nagarajaiah, 2015). The latter is achieved by exploiting the signal's *sparsity* information (i.e., the non-zero signal coefficients) on an orthonormal basis (e.g., Donoho, 2006). Therefore, CS techniques may also lead to simpler and cheaper sensors. However, in all CS approaches reported in the literature, the response acceleration signals are treated as deterministic, which is not in line with the assumption of white-noise excited structural systems, while a certain level of sparsity is assumed for measured signals. Further, computationally expensive signal reconstruction from the compressed measurements is required after transmission. In CS, sparse recovery is a computationally intensive problem that strongly depends on the sparsity attributes of the measured signals on a pre-defined vector basis. However, this sparsity information is unknown in real-time VSHM deployments, and it is adversely affected by noisy environments encountered in practice (e.g., Bao et al., 2011; O'Connor et al., 2014; Huang et al., 2016). Such knowledge of the signal sparsity attributes can be gained in advance using different approaches. For example, the underlying signal sparsity can be derived from allowing the two-way communication between the wireless sensors and the server during signal compression/acquisition (e.g., Klis and Chatzi, 2017). Such information can be also estimated via a small network of judicially located wired sensors sampling in the conventional manner (i.e., uniformly in time-domain at the Nyquist rate or above) and operating concurrently with an extensive CS-based wireless sensor network (e.g., Klis and Chatzi, 2015). However, both these approaches add complexity to OMA installation and increase the overall cost. Alternatively, a conservative sparsity level can be assumed on the measured acceleration response signals which increases post-processing computational demand and reduces signal compressibility (e.g., Gkoktsi and Giaralis, 2017).

To circumvent the above CS limitations, a sub-Nyquist spectral estimation strategy is proposed by Gkoktsi and Giaralis (2019) as a viable alternative for power-efficient wireless sensor networks in VSHM applications. The proposed strategy is a signal-agnostic method that is not limited by sparsity constraints. It is based on PSBS techniques (see also Leus and Arianananda, 2011) together with a *deterministic* non-uniform in time-domain sampling scheme, known as *multi-coset sampling*, which can be implemented by utilising M interleaved analog-to-digital converter units, each operating N times slower than the Nyquist rate ($M <$

N). Ultimately, this approach can retrieve auto/cross power spectral estimates of non-sparse wide-sense stationary random signals (i.e., stochastic processes) directly from compressed measurements, bypassing the computationally demanding signal reconstruction operations in time-domain. This is achieved based on a weighted least-square optimisation criterion (e.g., Tausiesakul and González-Prelcic, 2013) which mathematically defines an *overdetermined* system of linear equations that can be easily solved. Section 2 presents the mathematical details of this approach, termed hereafter as *multi-sensor PSBS-based OMA* method. Its performance in extracting quality modal estimates is numerically evaluated in Section 3 using field-recorded data acquired from an existing bridge in Switzerland. Finally, Section 4 summarises concluding remarks.

2. Theoretical background

2.1 Multi-coset sampling

Let $x(t)$ be a continuous in time t, real-valued wide-sense stationary random signal (or stochastic process) characterised in the frequency domain by a power spectrum band-limited by $2\pi/T_s$. According to the multi-coset sampling strategy (e.g., Ariananda and Leus, 2012), the uniform grid of Nyquist sampled measurements $x[n] \in \mathbb{R}^N$, is first divided into K blocks of N consecutive samples. From each block $k = \{1, 2, \ldots, K\}$, a number of M samples ($M < N$) is selected at a deterministically pre-specified position which remains the same for all blocks. The acquired samples are governed by the sampling pattern sequence $\mathbf{s} = [s_0, s_1, \ldots, s_{M-1}]$ which further defines the pattern sequences $c_i[n]$ as

$$c_i[n] = \begin{cases} 1, & n = s_i \\ 0, & n \neq s_i \end{cases} . \tag{1}$$

In Equation (1), $i = \{0, 1, \ldots, M-1\}$ and $n = \{1-N, 2-N, \ldots, 0\}$ (i.e., in descending order). The signal compression level is defined by the compression ratio $CR = M/N$. In this manner, the multi-coset sampling strategy yields non-uniform in time-domain deterministic N-periodic samples. Figure 1 shows an example of the multi-coset sampling for $M = 3$, $N = 8$, $K = 4$ applied to a 32-long Nyquist sampled discrete time signal using the sampling pattern matrix $\mathbf{s} = [0, 2, 5]$ which leads to a signal compression at $CR = 3/8 = 37.5\%$. The above sampling strategy can be implemented by utilising M interleaved channels of analog-to-digital converter units operating at a sampling rate $1/(NT_s)$, (i.e., N times slower than the Nyquist rate $1/T_s$) (e.g., Arianandа and Leus, 2012).

2.2 Auto/cross power spectral estimation of sub-Nyquist measurements

Consider next a network of D identical multi-coset sub-Nyquist sampling devices, each consisted of M channels and operating under the same sampling pattern across their channels. The considered wireless sensor network is assumed to be placed along a structure, measuring D acceleration responses under ambient vibration. Let $x_a[n]$, $x_b[n]$ ($a, b = \{1, 2, \ldots, D\}$) be the unknown discrete-time sequences sampled at Nyquist rate from the band-limited, continuous in time-domain, acceleration response random signals $x_a(t)$ and $x_b(t)$, respectively. The ultimate goal of the multi-sensor PSBS approach is the recovery of the input cross-correlations

$$r_{x_a x_b}[p] = \mathrm{E}_x \{x_a[n] x_b[n-p]\} . \tag{2}$$

$r_{x_a x_b}$ are computed among all signals $x_a[n]$, $x_b[n]$ (i.e., input to the a, b devices), with $\mathrm{E}_\theta\{\cdot\}$ denoting the mathematical expectation operator with respect to a variable θ.

As illustrated in Figure 2, the above goal can be achieved through the acquisition of $M \times D$ output/compressed sequences $y_{i,a}[k]$, $y_{j,b}[k]$ from all $i, j \in \{0, 1, \ldots, M-1\}$ channels of the a, b devices, using the multi-coset sampling strategy detailed in Section 2.1. By collectively processing the acquired compressed measurements, the output cross-correlations can be computed as

$$r_{y_{i,a}, y_{j,b}}[l] = \mathrm{E}_y \left\{ y_{i,a}[k] y_{j,b}[k-l] \right\}, \tag{3}$$

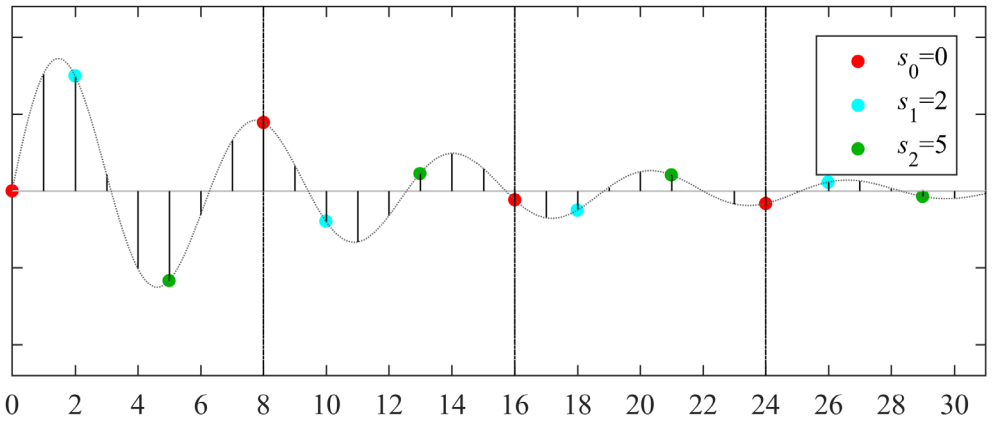

Figure 1: Example of multi-coset sampling applied to a 32-long Nyquist sampled discrete-time signal with M = 3, N = 8, K = 4, and sampling pattern $\mathbf{s}$ = [0, 2, 5].

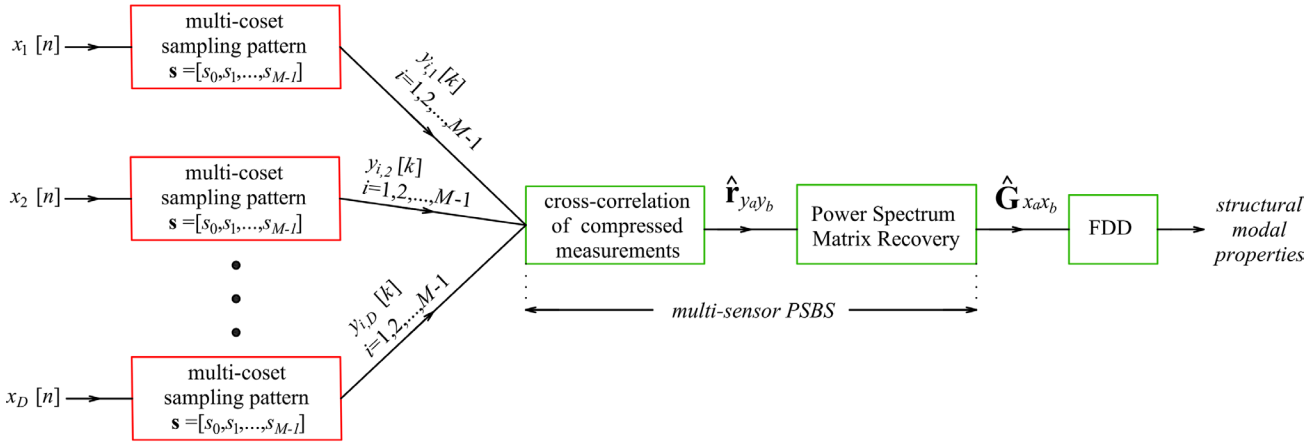

Figure 2: Flowchart of multi-sensor PSBS method for OMA (Gkoktsi and Giaralis, 2017).

which are collected further in the output cross-correlation matrix $\mathbf{r}_{y_a y_b} \in \mathbb{R}^{M^2 \times D}$ given as

$$\mathbf{r}_{y_a y_b}[l] = \left[r_{y_{0,a}, y_{0,b}}[l] \cdots r_{y_{0,a}, y_{(M-1),b}}[l] \right. \\ \left. r_{y_{1,a}, y_{0,b}}[l] \cdots r_{y_{(M-1),a}, y_{(M-1),b}}[l] \right]^T. \quad (4)$$

The expression in Equation (5) is then employed, allowing to relate the output cross-correlation matrix $\mathbf{r}_{y_a y_b} \in \mathbb{R}^{M^2 \times D}$ (Equation 4) with the unknown input cross-correlation matrix $\mathbf{r}_{x_a x_b} \in \mathbb{R}^{N \times D}$

$$\mathbf{r}_{y_a y_b}[l] = \sum_{p=0}^{1} \mathbf{R}_c[p]\, \mathbf{r}_{x_a x_b}[l-p], \quad (5)$$

using the pattern cross correlation matrix $\mathbf{R}_c \in \mathbb{R}^{M^2 \times N}$

$$\mathbf{R}_c[l] = \left[\mathbf{r}_{c_0, c_0}[l] \cdots \mathbf{r}_{c_0, c_{M-1}}[l] \right. \\ \left. \mathbf{r}_{c_1, c_0}[l] \cdots \mathbf{r}_{c_{M-1}, c_{M-1}}[l] \right]^T. \quad (6)$$

$\mathbf{R}_c$ is populated with the cross-correlation functions of the multi-coset pattern sequences $c_i[n]$, $c_j[n]$ given as

$$r_{c_i c_j}[p] = \sum_{n=1-\overline{N}}^{0} c_i[n]\, c_j[n-p] = \delta[p-(s_i - s_j)], \quad (7)$$

where $\delta[\cdot]$ denotes the Dirac delta function (i.e., $\delta[p] = 1$ for $p = 0$, and $\delta[p] = 0$ for $p \neq 0$).

Using the discrete Fourier transform matrix $\mathbf{F}$, the unknown power spectrum density matrix of the D structural acceleration response signals can be estimated upon solving the following equation

$$\hat{\mathbf{G}}_{x_a x_b} = \mathbf{F}\left(\mathbf{R}_c^{\mathrm{T}} \mathbf{W} \mathbf{R}_c\right)^{-1} \mathbf{R}_c^{\mathrm{T}} \mathbf{W} \hat{\mathbf{r}}_{y_a y_b}, \quad (8)$$

where $\mathbf{W}$ is a weighting matrix, the superscript '–1' denotes matrix inversion, and '^' indicates the estimate of a variable (e.g., $\hat{\mathbf{G}}$).

3. Numerical assessment

The effectiveness of the multi-sensor PSBS approach (Figure 2) is numerically assessed against field-recorded data obtained from the Bärenbohlstrasse Overpass in Zürich, Switzerland (e.g., Chatzi and Spiridonakos, 2015; Spiridonakos et al., 2016) under operational loading. The considered bridge is 30.90 m long, having a deck of variable width, while it is nearly symmetric along the longitudinal axis. It consists of a solid prestressed concrete slab with two equal-length spans of 14.75 m each. The deck is supported through steel bearings on a double-column pier at mid-span and on the abutments. Horizontal movement of the deck is not allowed, apart from the longitudinal bridge direction at the southern abutment (right one in Figure 3). The soffit of the deck was instrumented by a network of 18 tethered sensors over a period of 12 months, recording vertical acceleration response signals with a sampling rate at 200 Hz (T_s = 0.005 s) for approximately 10 minutes/hour using a conventional uniform sampling scheme. A photo of the bridge and a sketch of the sensor's layout is shown in Figure 3. Further details regarding the bridge, the sensors' installation and data acquisition can be found in Chatzi and Spiridonakos (2015), and Spiridonakos et al. (2016).

In this study, a dataset of 18 vertical acceleration response signals is used, recorded on 19 June 2014 between 15:08:54 and 15:17:51; it comprises 107460 samples per sensing location, conventionally (i.e., uniformly) sampled at 200 Hz. The considered dataset was recorded under ambient wind and traffic dynamic loads that excite the first few modes of the monitored bridge. Aiming to remove the mean value and any potential low-frequency trend within each acceleration response signal, the acquired raw data are first processed with a 4th-order Butterworth bandpass filter in the frequency range of 0.15–50 Hz. Notably, the upper cut-off frequency at 50 Hz is determined by the sensors' anti-aliasing filter which defines a Nyquist sampling frequency at 100 Hz. The 18 'corrected' acceleration response signals are next compressively sampled at a high-signal compression level pertaining to a compression ratio of CR = 11% (i.e., 89% fewer samples compared to the

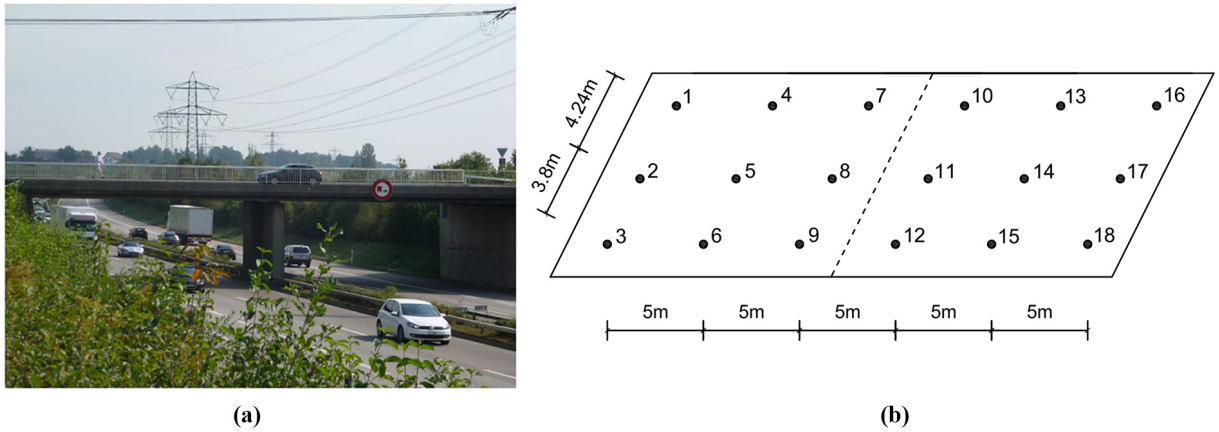

(a) (b)

Figure 3: (a) Bärenbohlstrasse Overpass in Zürich, Switzerland; (b) layout of the 18 sensors recording vertical acceleration responses under ambient excitation (Gkoktsi and Giaralis, 2017).

conventionally acquired/non-compressive samples) using the deterministic multi-coset sub-Nyquist sampling pattern by Tausiesakul and González-Prelcic (2013) for $M = 14$ and $N = 128$ ($CR = M/N$ =11%). These values are associated with a multi-coset sampler comprising $M = 14$ channels, each sampling acceleration response signals uniformly in time-domain with a rate of $N = 128$ times slower than the conventional sampling rate. The adopted sampling pattern is $\mathbf{s} = [0, 1, 2, 6, 8, 20, 29, 38, 47, 50, 53, 60, 63, 64]^{\mathrm{T}}$ (see also Gkoktsi and Giaralis, 2017; 2019). The acquired compressed acceleration measurements are subsequently collectively processed as detailed in Section 2.2, and the cross-spectrum matrix $\hat{\mathbf{G}}_{x_a x_b}$ in Equation (8) is computed for the 18 compressed bridge acceleration responses using a frequency resolution $\Delta f \simeq 0.03$ Hz. The recovered cross-spectrum matrix $\hat{\mathbf{G}}_{x_a x_b}$ is then treated by the standard FDD OMA algorithm (Brincker and Ventura, 2015), and it is decomposed to its singular values and vectors as expressed below:

$$\hat{\mathbf{G}}_{x_a x_b} = \mathbf{U}\Sigma\mathbf{V}^{\mathrm{T}}. \tag{9}$$

In Equation (9), $\mathbf{\Sigma}$ is a diagonal positive semi-definite matrix consisted of the singular values Σ_{rr} which carry the information of structural resonant (natural) frequencies f_r at the R excited modes of vibration (i.e., $r = \{1, 2, \ldots, R\}$). Furthermore, $\mathbf{U}$ and $\mathbf{V}$ are the unitary singular matrices holding the left and right singular vectors, respectively. The left singular vector $\mathbf{U}$ provides valid estimates of the mode shapes $\hat{\varphi}_r$, related to the estimated frequencies $\hat{f}_r$ of the dominant singular values (e.g., Brincker and Ventura, 2015).

For the proposed multi-sensor PSBS approach at CR = 11%, Figure 4 plots the derived first singular values vector, normalised to the maximum amplitude and plotted against the conventional/non-compressive FDD at uniform sampling rate (i.e., at CR = 100%). It is readily observed that the proposed sub-Nyquist approach can closely trace the first singular values vector obtained from the non-compressive FDD, identifying the same relative amplitudes across the considered frequency range. It is seen that the highest singular value amplitudes occur at 7.6 Hz and 11.7 Hz, associated with the 1st and 3rd resonant frequencies of the monitored bridge, respectively. Relatively smaller amplitudes occur at 10.4 Hz and 12.6 Hz, associated with the bridge natural frequencies at the less excited 2nd and 4th vibration modes, respectively. The extracted mode shapes of the bridge are presented in Figure 5, pertaining to the first two bending (Figures 5a to 5d) and two torsional (Figures 5e to 5h) modes of vibration. These are obtained from (*i*) the standard FDD method using the 18 conventionally acquired signals (each consisted of N = 107460 samples), and (*ii*) the PSBS-based approach at CR = 11%. From a qualitative point of view, Figures 5a to 5h confirm that the PSBS-

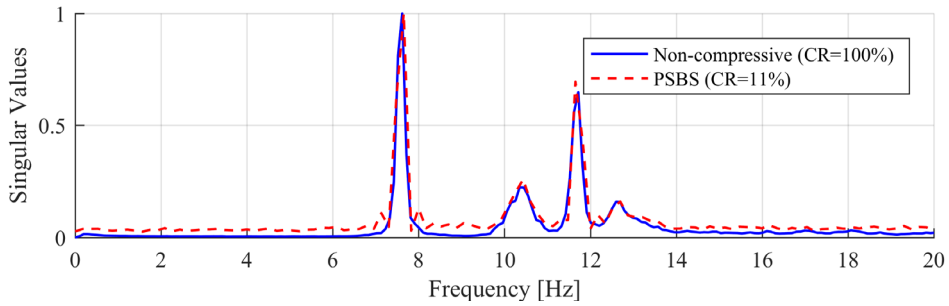

Figure 4: (a) First singular values vector of the bridge response spectrum matrix obtained from the non-compressive FDD (CR = 100%) and the multi-sensor PSBS (CR = 11%) approaches.

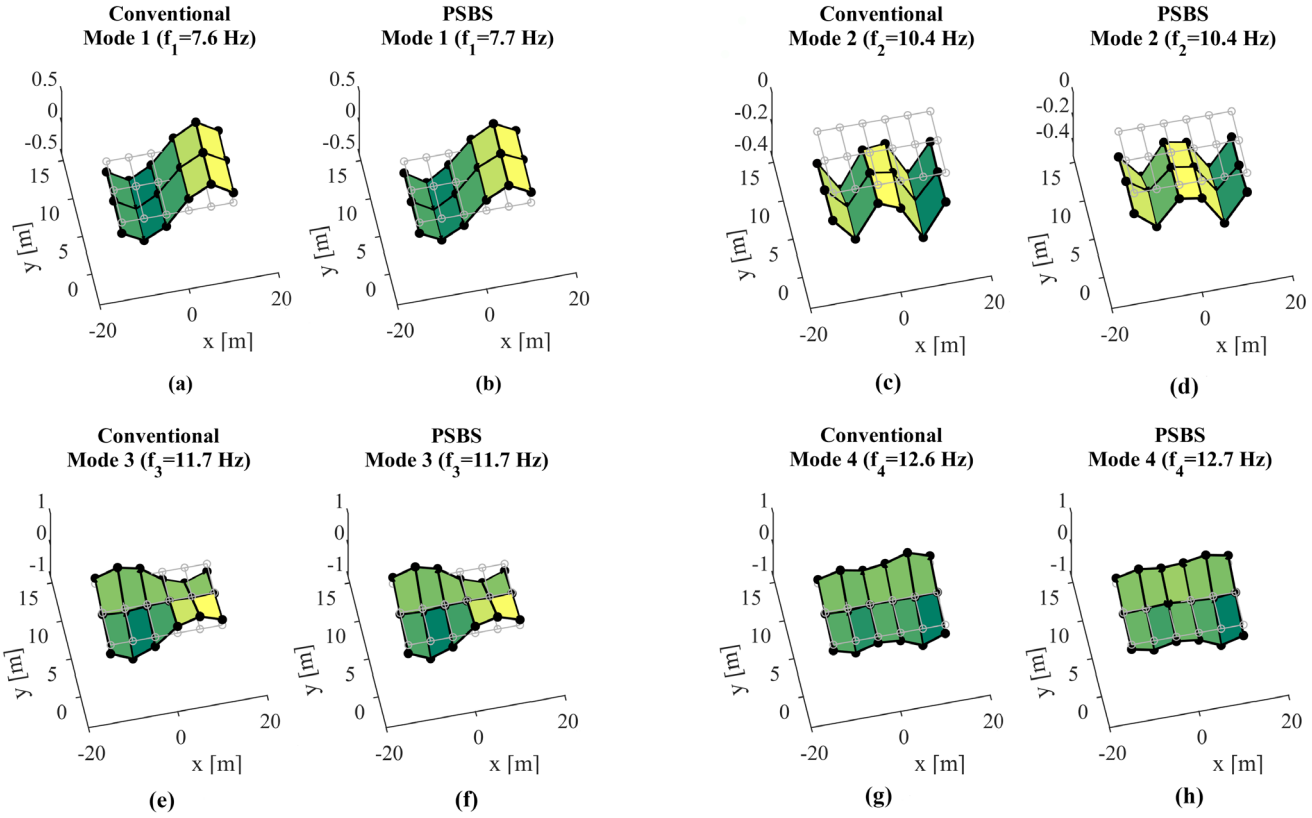

Figure 5: Estimation of mode shapes in Bärenbohlstrasse Overpass using conventional/non-compressive FDD and the multi-sensor PSBS-based FDD at *CR* = 11% (Gkoktsi and Giaralis, 2017).

based approach can extract the excited bridge mode shapes from highly compressed signals (*CR* = 11%) equally well with conventional approaches at uniform sampling rates (at Nyquist rate or above).

To quantify the level of accuracy for the estimated mode shapes, the *modal assurance criterion* (MAC) is employed (e.g., Brincker and Ventura, 2015), which measures the correlation between two mode shape vectors, taking values between 0 (uncorrelated) and 1 (fully correlated). MAC values obtained from the multi-sensor PSBS approach are plotted in Figure 6 for the four estimated mode shapes of the bridge. Figure 6 illustrates further a threshold MAC value at 0.9 (dashed black line); this quantity is commonly used as a criterion for checking the validity of the estimated mode shapes (i.e., MAC ≥ 0.9). Figure 6 superimposes in addition the MAC values obtained from an alternative sub-Nyquist OMA method proposed by O'Connor et al. (2014), termed CS-based approach. The O'Connor et al. approach relies on the theory of compressive sensing (e.g., Donoho, 2006) and depends on the sparsity information of the measured acceleration response signals. However, sparsity information is practically unknown while it is adversely affected by noisy environments encountered in practice. The fairness of the comparison of the two alternative approaches (in relation to up-front and/or operational monitoring costs) is safeguarded by the fact that neither of the approaches consider on-sensor data processing before transmission, while no prior knowledge on the properties (i.e., the sparsity) of the acquired signals is assumed available. Instead, this study assumes the availability of sensors that acquire and transmit signals directly in the compressed domain supporting low-power wireless network sensors. Figure 6 confirms that the multi-sensor PSBS-based method provides mode shapes with MAC values approximately equal to unity at *CR* = 11%, outperforming in terms of accuracy the CS-based approach as it yields higher MAC values in all cases considered. Nonetheless, it is observed that the CS-based approach can provide quality

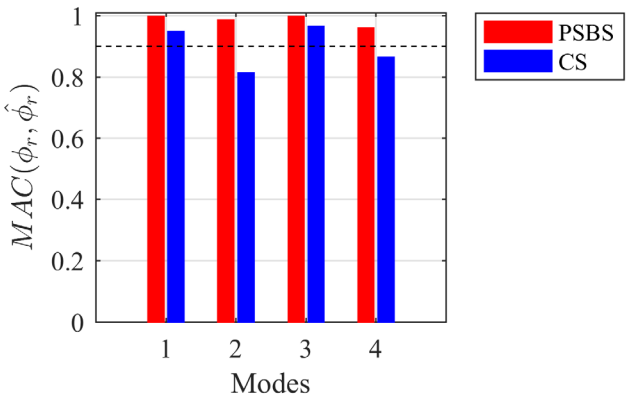

Figure 6: MAC employed in the case of the four excited vibration modes of the bridge obtained from the proposed multi-sensor PSBS approach and the CS-based FDD approach by O'Connor et al. (2014), at *CR* = 11%.

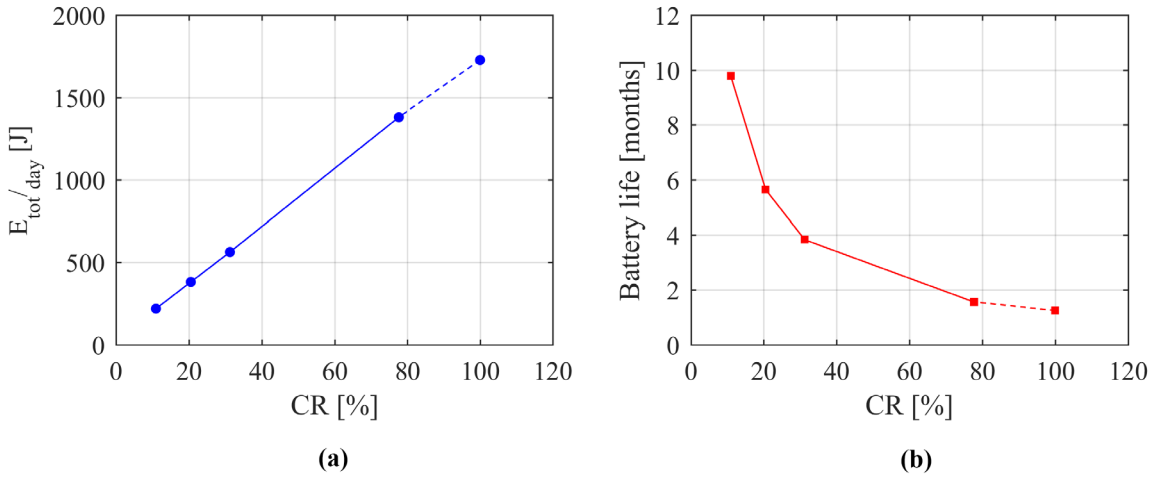

Figure 7: Estimates of (a) the total energy requirements, and (b) the battery life with respect to *CR* for the bridge case study (Gkoktsi and Giaralis, 2019)

mode shape estimates at the well-excited modes of vibration (i.e., Mode 1 and Mode 3) although it fails to retrieve the pertinent eigenvectors at the less excited modes (e.g., Mode 2 and Mode 4) resulting in MAC values below the threshold of 0.9.

Finally, the gains to the compression ratio, achieved by the multi-sensor PSBS-based approach, reflect analogously on energy savings in wireless sensor networks (e.g., Lynch, 2007; O'Connor et al., 2014). This is because wireless data transmission is by far the most power-hungry operation in wireless sensors, being directly related to the amount of data, *M*, transmitted from each sensor. In this respect, Figure 7 shows the daily energy savings of the bridge monitoring system based on the sampling rate reductions achieved by the developed multi-sensor PSBS-based approach at various signal compression levels (e.g., Gkoktsi and Giaralis, 2019). Energy consumption estimates are computed assuming a battery-operated smart wireless sensor operating at sub-Nyquist sampling rates for various *CR*s in the range of 10–100%. It is readily observed from Figure 7a that the total energy consumption, E_{tot}, decreases linearly at higher signal compression levels (i.e., at lower *CR*s). Figure 7b further confirms that the reduced energy consumption results in the elongation of battery lifetime which increases exponentially with lower *CR*s, leading to a more sustainable bridge monitoring system with reduced costs associated with maintenance and/or interruption of the normal operation of the monitored bridge.

4. Conclusions

This article presents a novel multi-sensor spectral estimation method for OMA, in support of smart wireless sensor technologies for energy-efficient VSHM in civil engineering structures. The proposed multi-sensor PSBS approach aims to reduce data transmission payloads by using the deterministic multi-coset sampling scheme. This is accomplished by considering compressed structural acceleration responses acquired at sub-Nyquist rates and wirelessly transmitted to a base station without any local (on-sensor) data processing. The adopted approach treats response acceleration signals as wide-sense stationary stochastic processes without imposing any signal sparsity conditions. It estimates the power spectrum density matrix of the acceleration signals by operating directly to the sub-Nyquist/compressed measurements at the base station. Then, the standard FDD algorithm for OMA is applied to the estimated power spectrum density matrix to extract structural mode shapes.

The performance of the proposed approach is numerically assessed with field-recorded bridge acceleration response signals acquired from an actual monitoring campaign in Zürich, Switzerland. Simulated compressed data are obtained at a high signal compression level at *CR* = 11% corresponding to 89% fewer measurements compared to non-compressive/conventional approaches (at Nyquist rate or above). It was numerically shown that the multi-sensor PSBS-based approach can accurately extract the first four mode shapes for the considered set of compressively sampled bridge acceleration signals. In fact, the multi-sensor PSBS-based approach yields MAC > 0.90 even for low-excited modes of vibration at *CR* = 11%, outperforming the recently proposed CS-based FDD approach by O'Connor et al. (2014). Overall, the numerical results demonstrate that the inherent signal agnostic attributes of the multi-sensor PSBS-based approach render this method advantageous compared to the CS-based approach in OMA applications where high signal compression levels are desired to address sensor power consumption and wireless bandwidth transmission limitations. Finally, it was shown that the consideration of signal compressive techniques at *CR* values as low as 11% leads to drastic reductions in individual sensor energy demands, and therefore to considerable increase of battery life expectancy, enhancing the sustainability of OMA monitoring systems.

Acknowledgments

This work is part of the author's PhD research supervised by Dr Agathoklis Giaralis whose contribution is gratefully acknowledged. The author further acknowledges the support of City, University of London through a PhD studentship. Special thanks are given to the EPSRC project pattern, Dr Bamrung Tausiesakul (University of Vigo), and Professor Eleni Chatzi (ETH, Zürich) for providing field-recorded acceleration data for the Bärenbohlstrasse Overpass.

References

Arianandа, D. D., & Leus, G. (2012). Compressive wideband power spectrum estimation. *IEEE Transactions on Signal Processing*, **60:** 4775–4789.

Bao, Y., Beck, J. L., & Li, H. (2011). Compressive sampling for accelerometer signals in structural health monitoring. *Structural Health Monitoring*, **10:** 235–246.

Brownjohn, J. M. W. (2007). Structural health monitoring of civil infrastructure. *Philosophical Transactions of the Royal Society A: Mathematical, Physical and Engineering Sciences*, **365:** 589–622.

Brincker, R., & Ventura, C. E. (2015). *Introduction to Operational Modal Analysis*. John Wiley & Sons, Ltd, Chichester, UK.

Chatzi, E. N., & Spiridonakos, M. D. (2015). Incorporating uncertainty in vibration-based monitoring and simulation. In: Kruis, J., Tsompanakis, Y., & Topping, B. H. V. (Eds.) *Computational Techniques for Civil and Structural Engineering*, Saxe-Coburg Publications, Stirlingshire, UK, 175–198.

Donoho, D. L. (2006). Compressed sensing. *IEEE Transactions on Information Theory*, **52:** 1289–1306.

Gkoktsi, K., & Giaralis, A. (2017). Assessment of sub-Nyquist deterministic and random data sampling techniques for operational modal analysis. *Structural Health Monitoring*, **16:** 630–646.

Gkoktsi, K., & Giaralis, A. (2019). A multi-sensor sub-Nyquist power spectrum blind sampling approach for low-power wireless sensors in operational modal analysis applications. *Mechanical Systems and Signal Processing*, **116:** 879–899.

Huang, Y., Beck, J. L., Wu, S., & Li, H. (2016). Bayesian compressive sensing for approximately sparse signals and application to structural health monitoring signals for data loss recovery. *Probabilistic Engineering Mechanics*, **46:** 62–79.

Klis, R., & Chatzi, E. N. (2015). Data recovery via hybrid sensor networks for vibration monitoring of civil structures. *International Journal of Sustainable Materials and Structural Systems*, **2:** 161–184.

Klis, R., & Chatzi, E. N. (2017). Vibration monitoring via spectro-temporal compressive sensing for wireless sensor networks. *Structures and Infrastructures Engineering: Maintenance, Management, Life-Cycle Design and Performance*, **13:** 195–209.

Leus, G., & Arianandа, D. D. (2011). Power spectrum blind sampling. *IEEE Signal Processing Letters*, **18:** 443–446.

Lynch, J. P. (2007). An overview of wireless structural health monitoring for civil structures. *Philosophical Transactions of the Royal Society A: Mathematical, Physical and Engineering Sciences*, **365:** 345–372.

O'Connor, S. M., Lynch, J. P., & Gilbert, A. C. (2014). Compressed sensing embedded in an operational wireless sensor network to achieve energy efficiency in long-term monitoring applications. *Smart Materials and Structures*, **23:** 085014.

Park, J. Y., Wakin, M. B., & Gilbert, A. C. (2014). Modal analysis with compressive measurements. *IEEE Transactions on Signal Processing*, **62:** 1655–1670.

Spiridonakos, M. D., Chatzi, E. N., & Sudret, B. (2016). Polynomial chaos expansion models for the monitoring of structures under operational variability. *ASCE–ASME Journal of Risk and Uncertainty in Engineering Systems*, Part A: Civil Engineering, **2:** B4016003.

Tausiesakul, B., & González-Prelcic, N. (2013). Power spectrum blind sampling using minimum mean square error and weighted least squares. *IEEE Record of the 47th Asilomar Conference on Signals, Systems and Computers*, Pacific Grove, CA, USA, 153–157.

Yang, Y., & Nagarajaiah, S. (2015). Output-only modal identification by compressed sensing: Non-uniform low-rate random sampling. *Mechanical Systems and Signal Processing*, **56–57:** 15–34.

Revisiting the Basis for Viscous Damping in Seismic Analysis

Andreas H. Nielsen
Atkins, Glasgow, UK

1. Introduction

It is widely known that the acceleration ordinate on a response spectrum graph can be either 'true' or 'pseudo-' acceleration, with the true acceleration defined as the maximum absolute total acceleration and the pseudo-acceleration defined as the maximum absolute relative displacement multiplied by circular frequency squared. The two quantities are almost equal over a wide frequency range, diverging only at low frequencies and with increasing levels of viscous damping. In the author's experience, textbooks in earthquake engineering tend to use pseudo-acceleration while many academic papers tend to use true acceleration. Practitioners seldom declare which quantity they are using. This laissez-faire approach is perhaps explained by the fact that the numerical difference between two quantities is rarely of any significance. There is, however, an elementary difference between the two quantities that is not widely appreciated, and this difference was the topic of a paper published by the author (Nielsen, 2018). An abbreviated and somewhat modified version of the paper is reproduced below. The article is aimed at students, graduates, young practitioners and other newcomers to the field who may be interested in the theoretical foundations of seismic analysis.

2. The interpretation problem

Viscous damping in numerical analysis is a convenient model that can replicate several manifestations of energy dissipation observed in real situations such as decay of free vibration or limited response under steady state excitation at resonant frequencies. The model is remarkably successful in this regard; we know that the model is not underpinned by any physical laws when used to model inherent structural damping (it is a mathematical abstraction), but it enables us to predict the response of many real systems with satisfactory accuracy.

In the following, the discussion is focussed on the response of the classical single-degree-of-freedom (SDOF) system: a massless linear-elastic spring arranged in parallel with a viscous damper (also massless) connected to a discrete mass. The system contains two internal forces: one that is conservative (the spring force F_S) and one that is non-conservative (the damping force F_D). The total internal force ($F_R = F_S + F_D$) is in dynamic equilibrium with the externally applied force F_E and the inertial force F_I according to d'Alembert's principle. These basic considerations, which can be extended to multi-degree-of-freedom systems, are well understood and accepted.

For many engineering applications, we are interested in the peak force within the spring (the peak force being the maximum absolute value). The spring may represent a real spring, a single structural member such as a bar or a beam, or even a structure with multiple members. The peak spring force is evaluated from the displacement time history $w(t)$ as

$$F_{SP} = \max|F_S| = \max|kw|, \tag{1}$$

where k is the stiffness coefficient.

In general, the velocity is always zero at the instant of peak displacement, and so if F_{SP} occurs at a specific time, then $F_D = 0$ at the same time, and therefore F_{SP} is equal to the absolute difference of F_E and F_I at that instant in time ($|F_E - F_I|$). However, the peak difference of F_E and F_I ($\max|F_E - F_I|$) is not necessarily equal to F_{SP}. In fact, the peak internal force required to balance the peak difference of F_E and F_I is given by

$$F_{RP} = \max|F_S + F_D| = \max|kw + c\dot{w}|, \tag{2}$$

where c is the damping coefficient.

It is not immediately clear whether we ought to use F_{SP} or F_{RP} for assessment or design of the spring (or the member that it represents) within the context of force-based design. Two interpretations are possible. On one hand, we acknowledge that the viscous force is a mathematical abstraction, and that the force in the spring must satisfy Hooke's law, and on this basis we conclude that the peak force in the spring is equal to F_{SP} (this may be termed a *Hookean* interpretation – *ut tensio sic vis*). On the other hand, we acknowledge that to satisfy the principle of dynamic equilibrium at the critical instant in time, and to satisfy Newton's second law, we must provide a structural element capable of sustaining a dynamic force equal to F_{RP} (this may be termed a *Newtonian* interpretation – *mutationem motus proportionalem esse vi motrici impressae*). Which one is correct?

This question represents an elementary interpretation problem associated with viscous damping – a problem that has not received much attention within the literature to date. In the author's experience, the default interpretation is the Hookean. For example, when using the spectral

pseudo-acceleration for seismic design of structures, we have implicitly opted for a Hookean interpretation. If instead we were to use the true spectral acceleration, then we would have opted for a Newtonian interpretation. The spectral pseudo-acceleration is approximately equal to the true spectral acceleration for low levels of damping and over a broad range of frequencies. The difference between the two accelerations becomes significant only at frequencies below 0.1 Hz for systems with low levels of damping (Chopra, 2012). Therefore, for many linear-elastic systems with low levels of damping, the difference between the two models is not significant, and presumably we can use one or the other without having to justify our choice.

In his comprehensive textbook, Chopra (2012) aligns with the Hookean interpretation. He notes that it is "inappropriate to include the velocity-dependent damping force because for structural design the computed element stresses are to be compared with allowable stresses that are specified based on static tests on materials (i.e., tests conducted at slow loading rates)." This justification appears tenuous. It is not possible to separate stresses into a 'static' term and a 'dynamic' term on the assumption that only the former is comparable to a static test. This would be tantamount to assuming that the action of gravity is somehow different from the action of acceleration, which would contradict the equivalence principle established in the theory of general relativity.

Although the Hookean interpretation is far more common, there are cases where a Newtonian interpretation has been adopted (perhaps unintentionally so). In ANSYS, for example, the reaction forces at the base of the structure are calculated as the sum of viscous and spring forces (here, the term 'spring forces' is used in a general sense denoting the product of the stiffness matrix and the displacement vector). However, within a Hookean framework, the internal forces in the elements that connect to the base would be calculated purely as the spring forces. This highlights an inconsistency in the approach as the forces used for design of the foundation may be greater than the forces used for design of the first storey columns or walls. As discussed below, this discrepancy may be aggravated if Rayleigh damping is used.

A serious problem already investigated by several researchers arises when a viscous damping model is used in combination with inelastic material response (e.g., Priestley and Grant, 2005; Hall, 2006; Jehel et al., 2014). It is beyond the scope of this article to discuss the problems in depth; however, one example may provide an appreciation of the difficulties. Bernal (1994) showed that systems with massless or nearly massless degrees-of-freedom (DOF) can develop abnormally high damping forces upon the onset of yielding or other inelastic effects characterised by sudden changes in stiffness. The changes in stiffness cause sudden changes in velocity and hence abnormally high damping forces. Observing that the equilibrium at massless DOF should be static in nature, not only for elastic behaviour but in general, Bernal again opted for a Hookean interpretation and concluded that the damping forces computed there are spurious. One may counter that massless DOF are themselves a mathematical abstraction as no solid is without mass. However, the findings suggest that the combination of viscous dampers and inelastic elements in the same model requires particular care.

Perhaps on an instinctive level, the question is whether we place greater trust in the displacement or the acceleration as a predictor of real response. Choosing displacement, we opt for a Hookean interpretation; choosing acceleration, we opt for a Newtonian interpretation. In moving towards displacement-based design, the earthquake engineering community appears to have decided in favour of the former. One approach commonly known as direct displacement-based design (e.g., Priestley et al., 2007) requires that the viscous damping coefficient is calibrated such that a substitute linear-elastic SDOF system yields the same displacement as a nonlinear system with a suitably chosen hysteretic behaviour. Forces required for design of non-yielding elements such as the foundation are Hookean – i.e., calculated as secant stiffness times peak displacement. However, this approach seems to overlook the fact (already pointed out by Biggs, 1964) that the forces of the substitute system are not equal to those of the real system.

3. Examples

The original paper (Nielsen, 2018) provided two examples. The first example compared the response of a linear-elastic SDOF system to that of an inelastic SDOF system under sinusoidal excitation (based on the premise that the latter is representative of a real system). In this example, the damping coefficient c was calibrated to give equal energy dissipation at resonance ($\beta = 1$, where β indicates the ratio of excitation frequency to natural frequency). Three frequency ratios were examined ($\beta = 0.5$, 1, and 4). The results are shown in Figure 1 (units are not important). The example shows that, depending on our interest in the force-displacement graphs, one interpretation may appear more valid than the other. At relatively low excitation frequencies ($\beta = 0.5$), the difference between the spring force and the total force is negligible. At resonance ($\beta = 1$), the hysteretic loops of the 'real' system are better represented by the total force F_R (Newtonian interpretation). However, at relatively high excitation frequencies ($\beta = 4$), the total force tends to overshoot, and the peak force is more closely approximated by the spring force F_S (Hookean interpretation).

Another example considered a two-degree-of-freedom (2DOF) system subject to earthquake excitation. Rayleigh damping was used to model energy dissipation in the system. As is well known, Rayleigh damping is a combination of mass-proportional and stiffness-proportional damping. The presence of mass-proportional dampers in the model complicates the interpretation problem discussed above.

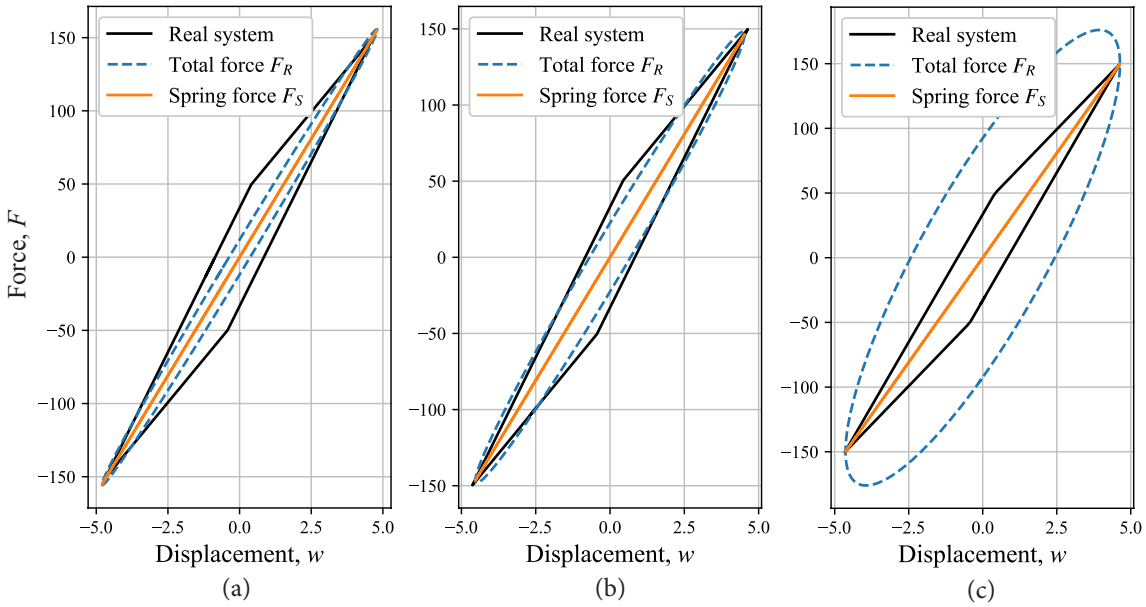

Figure 1: Response of bilinear and equivalent linear systems for (a) $\beta = 0.5$, (b) $\beta = 0.5$, and (c) $\beta = 4$.

To explain this, consider Figure 2. The system contains two subsystems designated primary (subscript p) and secondary (subscript s) as per convention. The peak force in the secondary spring is:

$$F_{s,SP} = k_s \max\left|w_s - w_p\right|. \tag{3}$$

When this peak force occurs, the viscous force in the secondary stiffness-proportional dashpot is zero. However, the viscous force in the mass-proportional dashpot is not necessarily zero. Therefore, the mass-proportional dashpot could influence the force in the spring depending on the relative phasing of the response.

On a more fundamental level, the mass-proportional dashpots provide an alternative load path to the foundation, bypassing the primary subsystem. This is not a problem within a Hookean interpretation where the viscous forces are ignored, but it clearly poses a problem within a Newtonian interpretation where the viscous forces are part of the load-resisting system.

A study was undertaken to quantify the difference between the two interpretations. Eight artificial accelerograms matching a typical design response spectrum were developed (Figure 3). The duration of each time history was 14 seconds.

The accelerograms were used as input to eight analyses of the 2DOF system shown in Figure 2. The fundamental system parameters are the natural frequency of the primary system f_p, the mass of the primary system m_p, and the damping ratios for the 1st and 2nd modes, ξ_1 and ξ_2. Three different values of f_p were considered (0.5, 2, and 6 Hz), the mass of the primary subsystem was given a value of unity, and the damping ratios were chosen as $\xi_1 = \xi_2 = 7\%$. The other system parameters are defined through the mass (R_m) and the frequency (R_f) ratios:

$$R_m = \frac{m_s}{m_p}, \tag{4}$$

$$R_f = \frac{f_s}{f_p}. \tag{5}$$

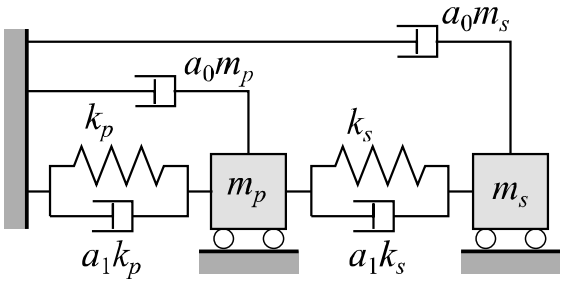

Figure 2: 2DOF system with Rayleigh damping.

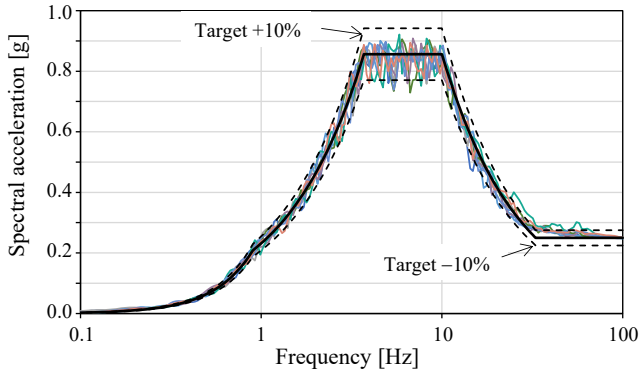

Figure 3: Target response spectrum at 5% damping and spectra from eight matching accelerograms.

Initially, the frequency of the primary system was chosen as f_p = 0.5 Hz, well into the displacement-sensitive region of the response spectrum. Eight transient analyses were carried out, using the input described above. The results from each analysis were peak dynamic reaction R_{RP} (including viscous forces) and peak primary spring force $F_{p,SP}$. The ratio of the latter to the former, $\rho_P = F_{p,SP}/R_{RP}$, was evaluated, and the mean of all eight analyses $\overline{\rho}_P$ was plotted as a function of R_f for five values of R_m. This process was repeated for f_p = 2 Hz (velocity-sensitive region) and f_p = 6 Hz (acceleration-sensitive region). The results are shown in Figure 4.

The results show that the mean force ratio $\overline{\rho}_P$ is consistently between 1 and 0.95 for $R_m \leq 1$, regardless of the primary subsystem frequency. Thus, when the secondary subsystem is lighter than the primary subsystem, the difference between the two approaches is insignificant. When the frequency of the primary subsystem is within the displacement-sensitive region, $\overline{\rho}_P$ may be less than 0.6 with high mass ratios – a situation that typifies base-isolated structures. However, when the frequency of the primary subsystem is within the acceleration-sensitive region, $\overline{\rho}_P$ is between 1 and 0.95 for $R_m \leq 100$.

The results lead to the conclusion that, except for certain cases where a low-frequency primary subsystem supports a relatively heavy secondary subsystem, the interpretation problem is mainly a theoretical problem with little relevance for practical design situations. However, this conclusion may not be valid for models with high levels of damping (say, $\xi > 10\%$) or for nonlinear models with viscous damping; for such models, it remains pertinent to validate the damping forces and to assess any major discrepancies between the spring force F_S and the total force F_R.

4. Concluding remarks and recommendations

This article examined the basis of viscous damping in seismic analysis. The article highlighted that analysts have a choice when they evaluate the internal forces in the structural elements: excluding or including the viscous forces. In the first case, the analyst subscribes to a Hookean interpretation, whereas in the second case, to a Newtonian interpretation. However, unless the structure contains a real viscoelastic material or viscous damping devices, the viscous damper is largely a mathematical artifice influencing both displacements and accelerations. Therefore, neither interpretation is strictly speaking correct, or both are

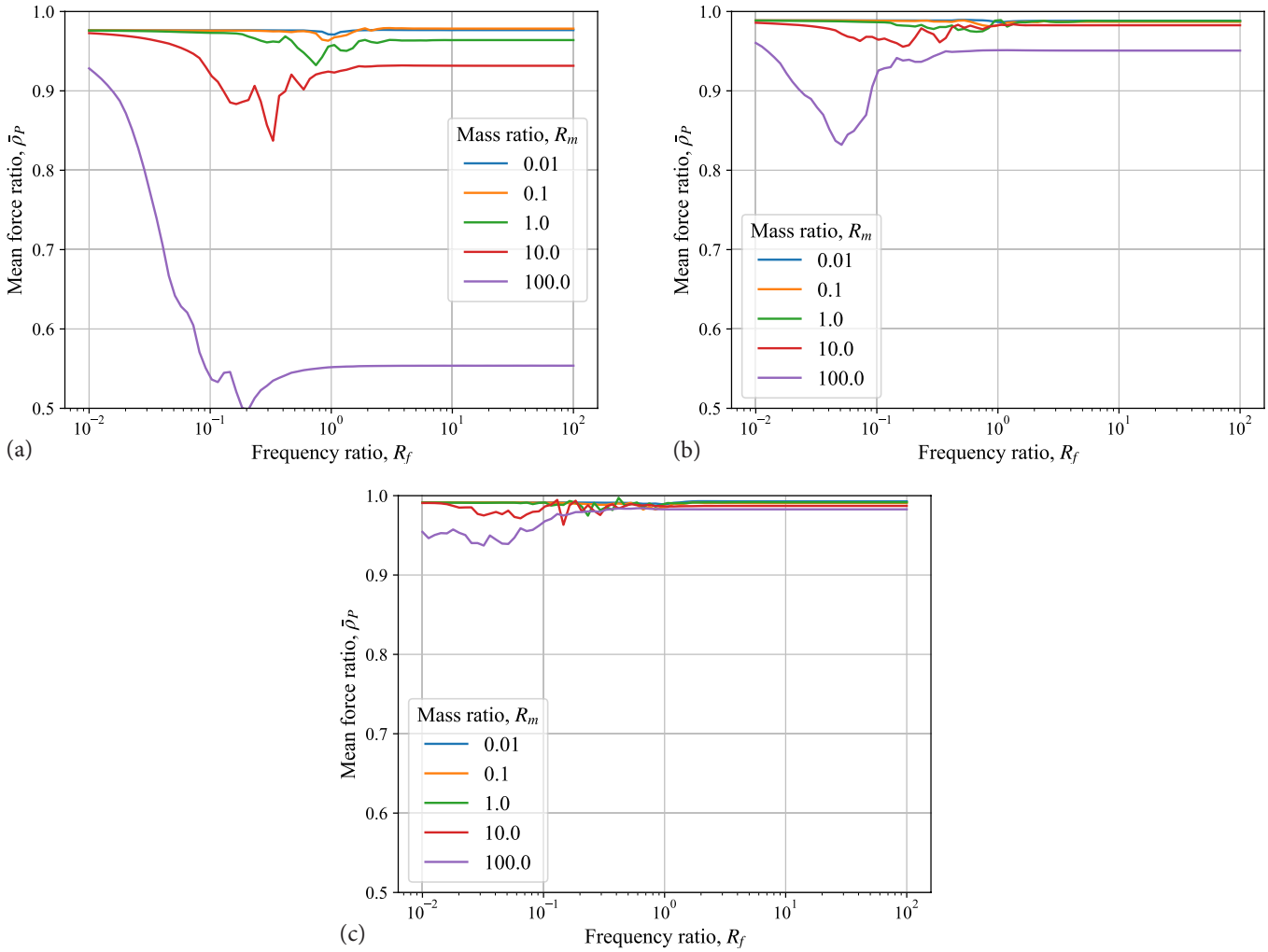

Figure 4: Mean force ratio for different primary subsystem frequencies: (a) f_p = 0.5 Hz; (b) f_p = 2 Hz; (c) f_p = 6 Hz.

equally correct, depending on your point of view.

In the context of force-based seismic design, whenever viscous damping is used to model inherent structural damping, it should be verified that the peak spring force is sufficiently close to the peak total force (the term 'force' should be understood in a general sense as covering not only forces but also moments and stresses). This ensures that internal forces in the structural elements are consistent with the relative displacements (the spring forces) and the total accelerations (the inertial forces). If significant differences are found, then the viscous damping should be reduced or eliminated from the model, and a more realistic material model should be implemented.

The findings of this article suggest that the following structural types may be unduly influenced by viscous damping:

- Structures responding in the displacement-sensitive range of the input spectrum (e.g., base-isolated structures).
- Structures supporting relatively large masses.
- Structures with rigid or nearly rigid body modes.
- Structures subject to high-frequency excitation (relative to their natural frequencies).
- Structures with yielding elements or other nonlinear effects in combination with viscous damping.

References

Bernal, D. (1994). Viscous damping in inelastic structural response. *ASCE Journal of Structural Engineering*, **120:** 1240–1254.

Biggs, J. M. (1964). *Introduction to Structural Dynamics*. McGraw-Hill, USA.

Chopra, A. K. (2012). *Dynamics of Structures: Theory and Applications to Earthquake Engineering (4th ed.)*. Prentice Hall, Upper Saddle River, NJ, USA.

Hall, J. F. (2006). Problems encountered from the use (or misuse) of Rayleigh damping. *Earthquake Engineering and Structural Dynamics*, **35:** 525–545.

Jehel, P., Léger, P., & Ibrahimbegovic, A. (2014). Initial versus tangent stiffness-based Rayleigh damping in inelastic time history seismic analyses. *Earthquake Engineering and Structural Dynamics*, **43:** 467–484.

Nielsen, A. H. (2018). Examining the basis for viscous damping in seismic analysis. *Proceedings of the 16th European Conference on Earthquake Engineering*, Thessaloniki, Greece.

Priestley, M. J. N., Calvi, G. M., & Kowalsky, M. J. (2007). *Displacement-Based Seismic Design of Structures*. IUSS Press, Pavia, Italy.

Priestley, M. J. N., & Grant, D. N. (2005). Viscous damping in seismic design and analysis. *Journal of Earthquake Engineering*, **9:** 229–255.

Notable Earthquakes September 2018 – December 2018

Reported by British Geological Survey

Issued by: Davie Galloway, British Geological Survey, February 2019.
Non British Earthquake Data supplied by: United States Geological Survey.

Year	Day	Mon	Time UTC	Lat	Lon	Dep km	Magnitude ML	Mb	Mw	Location
2018	05	SEP	18:07	42.69N	141.93E	35			6.6	HOKKAIDO, JAPAN
At least 41 people killed, including 36 from several landslides in Atsuma, and around 680 injured in southern Hokkaido. Dozens of houses destroyed from the multiple landslides in the region and many roads damaged due to liquefaction.										
2018	06	SEP	15:49	18.47S	179.35E	671			7.9	FIJI ISLANDS REGION
2018	07	SEP	19:00	52.94N	2.02W	7	1.5			CRESSWELL, STAFFORDSHIRE
2018	09	SEP	19:31	10.02S	161.50E	68			6.5	SOLOMON ISLANDS
2018	10	SEP	04:19	31.75S	179.37W	115			6.9	KERMADEC ISLANDS
2018	14	SEP	03:05	50.16N	5.11W	1	1.1			PENRYN, CORNWALL
Felt Porkellis (2 EMS).										
2018	15	SEP	02:01	59.06N	7.89W	12	1.6			NW ISLE OF LEWIS
2018	15	SEP	18:39	54.57N	1.64W	24	3.1			NEWTON AYCLIFFE, DURHAM

Year	Day	Mon	Time UTC	Lat	Lon	Dep km	Magnitude ML	Mb	Mw	Location
2018	16	SEP	21:11	25.42S	178.20E	576			6.5	FIJI ISLANDS REGION
2018	25	SEP	13:42	50.19N	5.08W	1	1.4			PENRYN, CORNWALL
Felt Pencoys and Kergilljack (2 EMS).										
2018	25	SEP	17:54	53.54N	1.64E	14	2.3			SOUTHERN NORTH SEA
2018	26	SEP	13:02	58.97N	1.43E	23	2.8			CENTRAL NORTH SEA
2018	28	SEP	08:28	57.02N	4.95W	14	1.7			INVERGARRY, HIGHLAND
2018	28	SEP	10:02	0.26S	119.85E	20			7.5	SULAWESI, INDONESIA
At least 2,077 people killed, with 1,075 still missing, over 4,400 injured and some 68,450 houses either destroyed or damaged, leaving over 206,500 homeless, in Sulawesi. A tsunami with an estimated maximum wave height of 7m was observed in Palu. Damage estimated at $US911 million.										
2018	30	SEP	10:52	18.36S	178.06W	550			6.7	FIJI ISLANDS REGION
2018	07	OCT	00:11	20.03N	73.01W	24			5.9	HAITI
At least 18 people killed, 548 injured and some 18,000 houses either destroyed or damaged, mainly in the northwest region of the country.										
2018	10	OCT	18:44	7.45S	114.46E	9			6.0	BALI SEA, INDONESIA
Four people killed, 36 others injured and over 400 houses damaged in Sumenep, Situbondo, Jember and Probolinggo, East Java.										
2018	10	OCT	20:48	5.70S	151.21E	39			7.0	PAPUA NEW GUINEA
2018	10	OCT	23:16	49.29N	156.30E	20			6.5	KURIL ISLANDS
2018	12	OCT	14:21	51.66N	3.12W	7	2.4			NEWBRIDGE, CAERPHILLY
2018	13	OCT	11:10	52.86N	153.24E	461			6.7	SEA OF OKHOTSK
2018	16	OCT	01:03	21.74S	169.52E	17			6.5	LOYALTY ISLANDS
2018	22	OCT	05:39	49.26N	129.21W	10			6.5	VANCOUVER ISLAND, CANADA
2018	22	OCT	06:16	49.34N	129.29W	10			6.8	VANCOUVER ISLAND, CANADA
2018	22	OCT	06:22	49.30N	129.72W	10			6.5	VANCOUVER ISLAND, CANADA
2018	24	OCT	20:18	52.94N	3.91W	9	1.3			FFESTINIOG, GWYNEDD
Felt Ffestiniog, Minffordd, Waunfawr, Cym-y-glo, Maentwrog, Trawsfynydd, Bethesda, Llanelltyd and Ganllwyd (3 EMS).										
2018	25	OCT	22:54	37.52N	20.56E	14			6.8	IONIAN SEA
2018	29	OCT	11:30	53.79N	2.96W	2	1.1			BLACKPOOL, LANCASHIRE
Felt Blackpool (2 EMS).										
2018	29	OCT	21:08	57.67N	6.25W	12	2.0			SKYE, HIGHLAND
Felt Gedintailor, Skye (2 EMS).										
2018	09	NOV	01:49	71.63N	11.24W	10			6.7	JAN MAYEN ISLAND
2018	09	NOV	22:05	53.11N	3.13W	9	1.5			TREUDDYN, FLINTSHIRE
2018	12	NOV	23:05	52.23N	2.72W	14	2.3			LEOMINSTER, HEREFORDSHIRE
Felt Church Stretton (2 EMS).										
2018	18	NOV	20:25	17.87S	178.93W	540			6.8	FIJI ISLANDS REGION
2018	19	NOV	05:23	54.56N	1.89W	12	1.7			BARNARD CASTLE, DURHAM
2018	22	NOV	18:05	54.25N	0.23W	1	2.1			FILEY, NORTH YORKSHIRE
2018	25	NOV	16:37	34.36N	45.74E	18			6.3	IRAN/IRAQ BORDER
One person killed and 43 others injured in Kalar, Iraq, and over 700 others injured and many buildings damaged in Sarpol-e Zahab, Iran.										

Year	Day	Mon	Time UTC	Lat	Lon	Dep km	Magnitude ML	Mb	Mw	Location
2018	30	NOV	17:29	61.35N	149.96W	47			7.0	ANCHORAGE, ALASKA
At least two people injured in Anchorage and damage to several buildings in Anchorage and										
2018	05	DEC	04:18	21.96S	169.42E	10			7.5	LOYALTY ISLANDS
2018	05	DEC	06:43	22.06S	169.73E	10			6.6	LOYALTY ISLANDS
2018	05	DEC	19:14	51.93N	0.69W	6	1.5			SOULBURY, BUCKINGHAMSHIRE
2018	11	DEC	02:26	58.54S	26.40W	133			7.1	SOUTH SANDWICH ISLANDS
2018	11	DEC	11:21	53.79N	2.96W	2	1.5			BLACKPOOL, LANCASHIRE
Felt Blackpool (2 EMS).										
2018	20	DEC	17:01	55.10N	164.70E	17			7.3	KOMANDORSKI ISLANDS
2018	26	DEC	13:06	54.93N	1.35W	8	1.6			SEABURN, TYNE & WEAR
2018	29	DEC	03:39	5.90N	126.92E	60			7.0	PHILIPPINES

Forthcoming Events

Evening Lectures

Annual General Meeting 2019

2 May 2019 (6:15 pm) at the
Institution of Civil Engineers, London

Agenda

All SECED members are invited to attend the Annual General Meeting (AGM) of the Society. Non-members are also welcome to attend, but will have no voting rights. AGM documents (agenda, minutes, Chairman's and Treasurer's report) should have been received by all SECED members (via email). The agenda is as follows.

1. APOLOGIES FOR ABSENCE
2. MINUTES OF THE AGM 2018
   To confirm the Minutes of the Annual General Meeting of 25th April 2018.
3. MATTERS ARISING
4. CHAIRMAN'S ANNUAL REPORT 2018/19
   Paul Doyle to report.
5. TREASURER'S REPORT AND MEMBERSHIP FEES
   Barnali Ghosh to report.
6. ELECTION TO THE COMMITTEE
   Results of nominations/elections to be reported.
7. ANY OTHER BUSINESS
8. DATE OF NEXT MEETING
   Wednesday 22 April 2020 at the Institution of Civil Engineers.

Any resolutions duly supported by not fewer than five members of the Society and notified to the Secretary at least seven days before the date of the Annual General Meeting, shall be dealt with at the meeting.

The SECED AGM is preceded by the Earthquake Engineering Field Investigation Team (EEFIT) AGM at 6pm.

Nominations

The following candidates have agreed to be nominated for the five vacancies on the SECED Committee:

- Hamid Ahmadi
- Guillermo Aldama-Bustos
- Fabio Freddi
- Damian Grant
- Angeliki Lessi-Cheimariou
- Andrew Mair
- Stergios Mitoulis

All members of the Society should have received a ballot form, which must be returned to the SECED Secretary before 4.30pm on Thursday 2nd May 2019. The results of the ballot will be announced at the AGM.

Further information

Tea, coffee and biscuits will be served between 5.30pm and 6pm.

Recovering the Lost 'Moment': How Timber-laced Masonry may Hold the Secret to Stopping Pancake Collapse of Concrete Moment Frames

Randolph Langenbach
2 May 2019 (6:30 pm) at the
Institution of Civil Engineers, London

Synopsis

Randolph Langenbach has become known for his research, writings, and consulting on earthquake risk and resilience of different types of traditional masonry construction. More recently his work has also focused on the increasing number of buildings of reinforced concrete and steel construction that have failed to live up to their promise of earthquake-safe performance; what he has observed in the resilience of some examples of traditional construction may provide important answers to this problem. In his SECED talk, Randolph will begin with his recent work in Nepal after the 2015 Gorkha earthquake. He will cover his observations on the performance of historic masonry buildings in Kathmandu including the 18th, 19th and 20th century wings of the Hanuman Dhoka Palace. Furthermore, he will present his work in the high-mountain and distant from roads countryside, where he has developed a proposal he named 'Gabion Bands'. The proposal provides a means for people to rebuild their houses with the only materials readily at hand: rubble stone with mud mortar together with bamboo, recycled timber, and sheet metal roofing. He will then go on to explore the problems of larger more contemporary moment-frame buildings with interior and exterior walls that are often consist of weak masonry. This masonry has often been ignored in their design, except for considering it as dead weight. His talk will reach back to the late 19th century in the USA with the invention of skeleton frame high-rise buildings. He will describe the many-decade efforts to separate the masonry infill walls from the frames, along with the more recent recognition of the need to embrace these walls as a strategic part of the engineering of these buildings (e.g., with confined masonry), without having to treat and calculate the masonry walls as shear walls. This discussion will include his concept called 'Armature Crosswalls'.

Randolph Langenbach

Randolph's background is closely tied to Britain, as he was an exchange student at Dulwich College, and later attended a post-graduate diploma course in Building Conservation at IAAS in York. He has two degrees, including a Master of Architecture, from Harvard. He was an Assistant Professor of Architecture at University of California, Berkeley, and more recently served as a Senior Analyst at the Federal Emergency Management Agency (FEMA). In 2003, he was awarded a Rome Prize Fellowship in honor of both his earthquake research and photography at the American Academy in Rome. His publications and biography can be found at www.conservationtech.com.

Further information

This evening meeting is organised by SECED and chaired by Edmund Booth (Edmund Booth Consulting Engineer). Non-members of the society are welcome to attend. Attendance at this meeting is free. Seats are allocated on a first come, first served basis. This meeting is preceded by the the EEFIT AGM (6pm), and the SECED AGM (6.15pm). Tea and biscuits will be served from 5.30pm to 6pm.

For up-to-date details and further information on events organised by SECED,
visit the SECED website or contact Shelly-Ann Russell (020 7665 2147, societyevents@ice.org.uk)

SECED Newsletter

The SECED Newsletter is published quarterly. Previous issues of the SECED Newsletter are available online. All contributions of relevance to the members of the Society are welcome.

Manuscripts should be sent by email. Diagrams, pictures and text should be attached in separate electronic files. Hand-drawn diagrams should be scanned in high resolution so as to be suitable for digital reproduction. Photographs should likewise be submitted in high resolution. Colour images are welcome.

Please contact the Editor of the Newsletter, Damian Grant, for further details.

This edition of the Newsletter was co-edited by Konstantinos Gkatzogias.

2019 SECED Conference

Earthquake risk and engineering towards a resilient world

9–10 September 2019 in Greenwich, London

Chair: Prof. Tiziana Rossetto

Overview

The SECED 2019 Conference will be a 2-day conference on Earthquake and Civil Engineering Dynamics taking place on 9–10 September 2019 in Greenwich, London. This is the first major conference to be held in the UK on this topic since the SECED 2015 Conference.

The conference will bring together experts from a broad range of disciplines, including structural engineering, nuclear engineering, seismology, geology, geotechnical engineering, urban development, social sciences, business and insurance; all focused on risk, mitigation and recovery.

The conference will take place in the modern facilities of the University of Greenwich (Stockwell Street Library building), with the conference dinner held in the Painted Hall of the Old Royal Naval College.

Please visit the SECED 2019 Conference website for further and updated information on conference keynote speakers, sessions, registration fees, key dates, sponsorships, conference committees, venue and accomodation.

University of Greenwich, Stockwell Street Library (© University of Greenwich)

Old Royal Naval College

Keynote speakers

SECED are delighted to announce the attendance of the following keynote speakers:

- Prof. Sinan Akkar, Boğaziçi University, Kandilli Observatory and Earthquake Research Institute, Turkey
- Prof. Ioannis Anastasopoulos, ETH Zurich, Switzerland
- Prof. Jack Baker, Stanford University, USA
- Prof. Eleni Chatzi, ETH Zurich, Switzerland
- Prof. Dina D'Ayala, University College London, UK
- Prof. Ahmed Elghazouli, Imperial College London, UK
- Zygmunt Lubkowski, Arup, UK

Conference sessions

The conference will feature a variety of sessions including:

- Blast, impact and vibration
- Catastrophe risk modelling for earthquakes
- Design for nuclear facilities
- Earthquake disaster risk reduction, reconnaissance and recovery
- Earthquake fragility and vulnerability
- Earthquake-triggered hazards and their impact
- Geotechnical earthquake engineering
- Induced seismicity
- Infrastructure system resilience
- Risk assessment in developing countries
- Seismic assessment and retrofitting
- Seismic design and analysis
- Seismic hazard and engineering seismology
- Seismic protective devices
- Soil–structure interaction
- Vibration serviceability

Key dates

- Paper submission closes: 30 May 2019

The Painted Hall (© University of Greenwich)

Registration fees	Discounted rates[1]		Standard rates[2]	
	Full (2 days)[3]	Day[4]	Full (2 days)[3]	Day[4]
Member	£440	£220	£485	£245
Non member	£485	£245	£550	£275
Student / retiree	£275	£140	£325	£165
Conference dinner ticket	£130		£130	

1. Discounted rates apply for registration on or before 11 July 2019.
2. The standard rates apply for registration after 11 July 2019.
3. The full rate includes one conference dinner ticket. Additional dinner tickets can be purchased for guests and accompanying family members.
4. The day rate excludes a conference dinner ticket.

Registration

Registration for the SECED 2019 Conference is now open. To register visit the Registration webpage; information on cancellation and substitution policies are also provided.

The *full registration* fee includes:
- 2-day conference sessions (9 & 10 September 2019)
- Conference bag including printed programme and USB proceedings
- Coffee breaks & light lunches
- One conference dinner ticket
- Paper submission (no additional cost for submission of one or more papers)

The *day registration* fee includes:
- 1-day conference sessions (9 or 10 September 2019)
- Conference bag including printed programme and USB proceedings
- Coffee breaks & light lunch on selected day
- Paper submission (no additional cost for submission of one or more papers)

Sponsorship and exhibition packages

More than 300 delegates from academia and industry are expected to attend the conference. *Sponsorship* packages have sold out, but if you are interested in a bespoke sponsorship opportunity, please contact Outsourced Events. One *exhibition space* remains available. For full terms and conditions, please contact seced@outsourcedevents.com.

The SECED 2019 Conference is sponsored by:

NORSAR JACOBS

ATKINS
Member of the SNC-Lavalin Group

MOTT MACDONALD ARUP

MMI Thornton Tomasetti

British Geological Survey
NATURAL ENVIRONMENT RESEARCH COUNCIL

Organisers

The SECED 2019 Conference is enabled by the Organising Committee and Outsourced Events.